



**HAL**  
open science

## A novel extrusion-based 3D bioprinting system for skeletal muscle tissue engineering

E Fornetti, F de Paolis, C Fuoco, S Bernardini, S Giannitelli, A Rainer, D Seliktar, C Gargioli, Frédérique Magdinier, J Baldi, et al.

► **To cite this version:**

E Fornetti, F de Paolis, C Fuoco, S Bernardini, S Giannitelli, et al.. A novel extrusion-based 3D bioprinting system for skeletal muscle tissue engineering. *Biofabrication*, 2023, 15 (2), pp.025009. 10.1088/1758-5090/acb573 . hal-03974646

**HAL Id: hal-03974646**

**<https://amu.hal.science/hal-03974646>**

Submitted on 16 Mar 2023

**HAL** is a multi-disciplinary open access archive for the deposit and dissemination of scientific research documents, whether they are published or not. The documents may come from teaching and research institutions in France or abroad, or from public or private research centers.

L'archive ouverte pluridisciplinaire **HAL**, est destinée au dépôt et à la diffusion de documents scientifiques de niveau recherche, publiés ou non, émanant des établissements d'enseignement et de recherche français ou étrangers, des laboratoires publics ou privés.



Distributed under a Creative Commons Attribution 4.0 International License



PAPER • OPEN ACCESS

## A novel extrusion-based 3D bioprinting system for skeletal muscle tissue engineering

To cite this article: E Fornetti *et al* 2023 *Biofabrication* **15** 025009

View the [article online](#) for updates and enhancements.

### You may also like

- [A biofabrication method to align cells within bioprinted photocrosslinkable and cell-degradable hydrogel constructs via embedded fibers](#)  
Margaret E Prendergast, Matthew D Davidson and Jason A Burdick
- [Manufacturing of self-standing multi-layered 3D-bioprinted alginate-hyaluronate constructs by controlling the cross-linking mechanisms for tissue engineering applications](#)  
Gopinathan Janarthanan, Jung Hyun Kim, Ingul Kim et al.
- [4D bioprintable self-healing hydrogel with shape memory and cryopreserving properties](#)  
Shin-Da Wu and Shan-hui Hsu

# Biofabrication



## PAPER

### OPEN ACCESS

RECEIVED  
27 June 2022

REVISED  
16 December 2022

ACCEPTED FOR PUBLICATION  
23 January 2023

PUBLISHED  
3 February 2023

Original content from this work may be used under the terms of the [Creative Commons Attribution 4.0 licence](https://creativecommons.org/licenses/by/4.0/).

Any further distribution of this work must maintain attribution to the author(s) and the title of the work, journal citation and DOI.



# A novel extrusion-based 3D bioprinting system for skeletal muscle tissue engineering

E Fornetti<sup>1</sup>, F De Paolis<sup>1,2</sup>, C Fuoco<sup>1</sup>, S Bernardini<sup>1</sup>, S M Giannitelli<sup>3</sup>, A Rainer<sup>3,4</sup>, D Seliktar<sup>5</sup>, F Magdinier<sup>6</sup>, J Baldi<sup>7</sup>, R Biagini<sup>7</sup>, S Cannata<sup>1</sup>, S Testa<sup>6,\*</sup> and C Gargioli<sup>1,\*</sup>

<sup>1</sup> Department of Biology, University of Rome ‘Tor Vergata’, Rome, Italy

<sup>2</sup> PhD Program in Cellular and Molecular Biology, Department of Biology, University of Rome ‘Tor Vergata’, Rome, Italy

<sup>3</sup> Department of Engineering, Università Campus Bio-Medico, Rome, Italy

<sup>4</sup> Institute of Nanotechnology (NANOTEC), National Research Council, Lecce, Italy

<sup>5</sup> Department of Biomedical Engineering, Techion Institute, Haifa, Israel

<sup>6</sup> Aix-Marseille University, INSERM, MMG, Marseille Medical Genetics, Marseille, France

<sup>7</sup> IRCCS Regina Elena National Cancer Institute, Rome, Italy

\* Authors to whom any correspondence should be addressed.

E-mail: [stefano.testa@univ-amu.fr](mailto:stefano.testa@univ-amu.fr) and [cesare.gargioli@uniroma2.it](mailto:cesare.gargioli@uniroma2.it)

**Keywords:** 3D bioprinting, skeletal muscle tissue engineering, muscle reconstruction, VML, PEG-fibrinogen

Supplementary material for this article is available [online](#)

## Abstract

Three-dimensional (3D) bioprinting is an emerging technology, which turned out to be an optimal tool for tissue engineering approaches. To date, different printing systems have been developed. Among them, the extrusion-based approach demonstrated to be the most suitable for skeletal muscle tissue engineering, due to its ability to produce and deposit printing fibers in a parallel pattern that well mimic the native skeletal muscle tissue architecture. In tissue bioengineering, a key role is played by biomaterials, which must possess the key requisite of ‘printability’. Nevertheless, this feature is not often well correlated with cell requirements, such as motives for cellular adhesion and/or absorbability. To overcome this hurdle, several efforts have been made to obtain an effective bioink by combining two different biomaterials in order to reach a good printability besides a suitable biological activity. However, despite being efficient, this strategy reveals several outcomes limitations. We report here the development and characterization of a novel extrusion-based 3D bioprinting system, and its application for correction of volumetric muscle loss (VML) injury in a mouse model. The developed bioprinting system is based on the use of PEG-Fibrinogen, a unique biomaterial with excellent biocompatibility, well-suited for skeletal muscle tissue engineering. With this approach, we obtained highly organized 3D constructs, in which murine muscle progenitors were able to differentiate into muscle fibers arranged in aligned bundles and capable of spontaneously contracting when cultured *in vitro*. Furthermore, to evaluate the potential of the developed system in future regenerative medicine applications, bioprinted constructs laden with either murine or human muscle progenitors were transplanted to regenerate the *Tibialis Anterior* muscle of a VML murine model, one month after grafting.

## 1. Introduction

In the last two decades, three-dimensional (3D) bioprinting has been widely employed in tissue engineering strategies. The possibility to build constructs with a spatially designed distribution of matrix and cells and the high reproducibility of these structures makes 3D bioprinting an excellent tool to produce

and study artificial tissues. The extrusion-based 3D bioprinting systems proved to be particularly effective in obtaining artificial skeletal muscle tissues [1]. The continuous and controllable deposition of printing fibers loaded with muscle progenitors and the possibility to arrange densely and evenly aligned fibers allows to reproduce the typical architecture of native skeletal muscle tissue, which is essential for the

tissue functionality [2]. Moreover, muscle progenitor cells within the printing fiber are forced to fuse and elongate along the printing direction by both the shear stress occurring in the printing nozzle and the confinement of cells in a limited space [3, 4]. As a result, this method allows generating highly organized artificial muscle constructs even in absence of external stimuli, such as mechanical stretching or electric stimulation. A key role is played by biomaterials in this process, in particular hydrogels, and their capability of transitioning from liquid to gel in a cell-safe manner. This quality, so called ‘printability’, is mainly dependent on the hydrogel viscosity and crosslinking time [5, 6]. Several biomaterials share these features and are employed in extrusion-based bioprinting. Widely employed hydrogels in tissue engineering are among others alginate [7], able to instantly polymerize upon bivalent ions exposure; chitosan [8], providing many biological properties including the ability to interact with cell membrane and controllable degradation; and collagen type I, known to improve cellular attachment and growth [9]. However, mentioned biomaterials own some limitations: while alginate is biologically inert and has a limited biodegradability, chitosan has a poor post-printing shape fidelity and collagen type I polymerizes at high temperatures and its complete gelation can take more than 30 min [10]. To overcome these hindrances, most of the current extrusion-based printing system are based on a combination of two biomaterials, one having appropriate printability (commonly alginate), which is crucial during the printing process, and the other with desirable biocompatibility (commonly fibrin-based hydrogels or gelatin), fundamental in sustaining the biological processes required for cell proliferation and differentiation [11, 12]. While demonstrating great efficiency in producing highly organized structures *in vitro*, this approach often requires removal of the printable material with chelating agents or specific enzymes to allow cellular physiological processes and *in vivo* integration [13].

PEG-Fibrinogen (PF) is a hybrid hydrogel obtained by the combination of PolyEthylene Glycol (PEG) with denatured fibrinogen molecules that already demonstrated to be an excellent biomimetic matrix for skeletal muscle tissue engineering both *in vitro* and *in vivo* [14–16]. In fact, this hydrogel is characterized by a high biocompatibility, being enriched with cell adhesion domains and proteolytic enzymes targets, which ensure its integration, remodeling and absorption *in vivo* [17]. However, the polymerization process for this photocurable hydrogel is hardly compatible with the concept of printability, occurring relatively long time of UV exposure for the transition from liquid to gel state [18].

Here we report an innovative extrusion-based 3D bioprinting system exploiting PF, which properties

demonstrated to be highly suitable for skeletal muscle differentiation. In particular, we developed a printing system able to drastically reduce the UV exposure time, allowing to use PF as bioink single component matrix. Moreover, this system presents a high resolution of the printing fibers (around 100  $\mu\text{m}$ ), a high efficiency in skeletal muscle differentiation and organization *in vitro*, and remarkable biocompatibility *in vivo*. All the bioprinter components were studied and optimized to obtain a 3D architecture closer as possible to the native organization of the skeletal muscle tissue, with bundles of fibers evenly oriented toward printing direction. The general morphology of the construct was maintained throughout the experimental time thanks to the special stainless-steel supports, specifically designed for the presented biotechnology.

The set-up for the printing system was conducted using a murine source of muscle progenitors, the mesoangioblast (Mabs), which possess high myogenic capabilities both *in vitro* and *in vivo* [14, 15]. Once demonstrated the validity of this system, a human source of muscle progenitors, the muscle-derived human mesenchymal stem cells (hMSCs) [19, 20] was tested in *in vivo* experiments, demonstrating that the described 3D bioprinting system could be a valuable tool for regenerative medicine approaches.

## 2. Materials and methods

### 2.1. Cell culture and bioink formulation

Mouse mesoangioblasts (Mabs) were transduced with third-generation lentiviral vectors encoding the reporter gene nuclear  $\beta$ -galactosidase (nLacZ) as previously described [14]. Cells were cultured on Petri dishes (Falcon) at 37 °C with 5% CO<sub>2</sub> in DMEM GlutaMAX (Gibco) supplemented with heat-inactivated 10% fetal bovine serum (Euroclone), penicillin (100 IU ml<sup>-1</sup>, Gibco), streptomycin (100 mg ml<sup>-1</sup>, Gibco). hMSCs were isolated from skeletal muscle biopsies following a protocol that involves mechanical mincing, enzymatic digestion with type II collagenase, filtration, and selection of the colonies on plastic surface at low confluence, as previously described [19]. Human progenitors were cultured on Petri dishes (Falcon) at 37 °C with 5% CO<sub>2</sub> in Cyto-Grow medium (Resnova) supplemented with penicillin (100 IU ml<sup>-1</sup>, Gibco) and streptomycin (100 mg ml<sup>-1</sup>, Gibco). Skeletal muscle biopsies were obtained from healthy donors following informed consent in line with the guidelines of the Helsinki declaration on Human rights.

For bioink formulation, muscular progenitors (Mabs or hMSCs) were resuspended to a final concentration of  $2 \times 10^7$  cells ml<sup>-1</sup> in a solution of PF, (8 mg ml<sup>-1</sup>) in phosphate buffered saline (PBS) and 0.1% w v<sup>-1</sup> Irgacure 2959 was added to the bioink

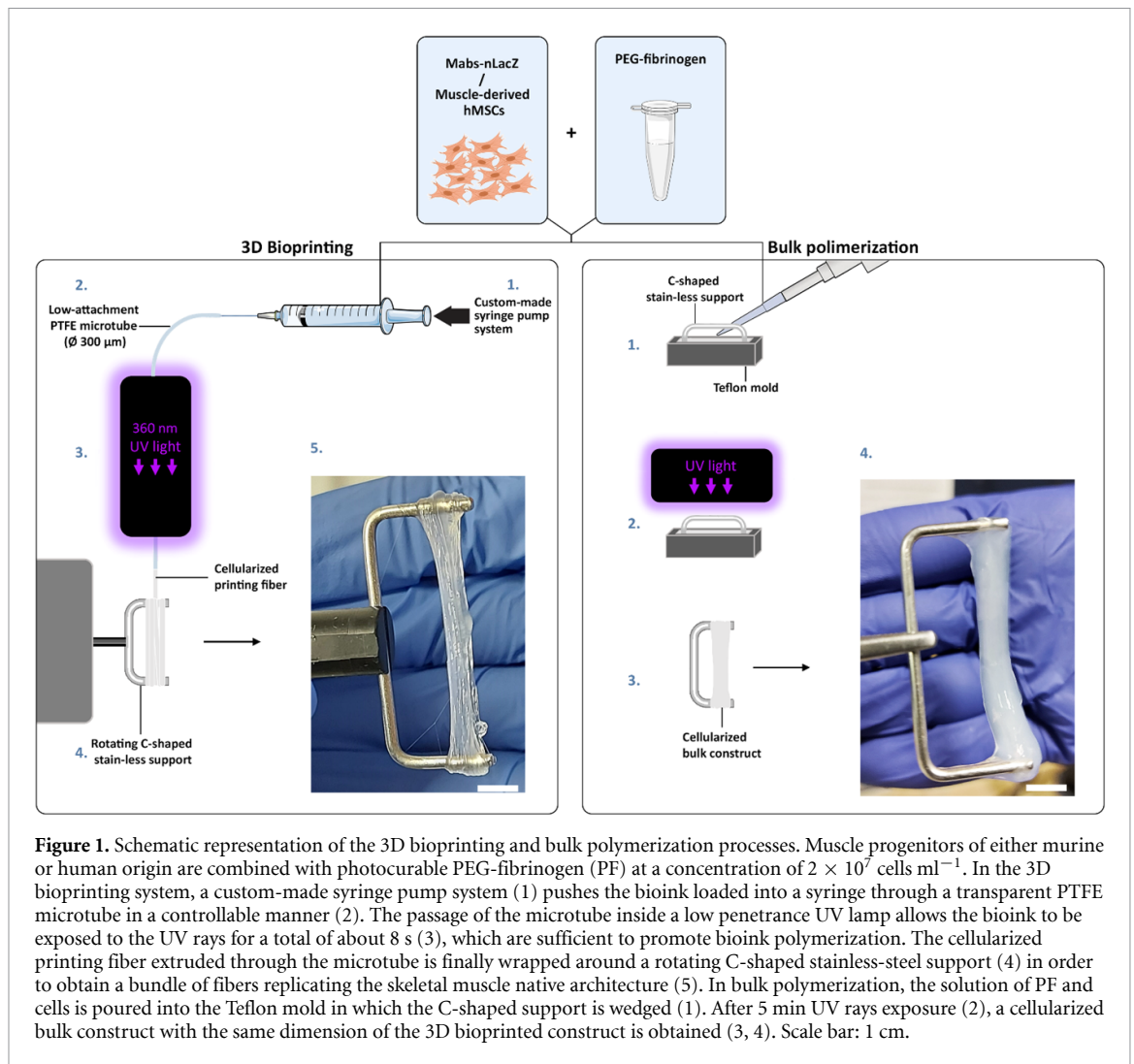


**Figure 1.** Schematic representation of the 3D bioprinting and bulk polymerization processes. Muscle progenitors of either murine or human origin are combined with photocurable PEG-fibrinogen (PF) at a concentration of  $2 \times 10^7$  cells  $\text{ml}^{-1}$ . In the 3D bioprinting system, a custom-made syringe pump system (1) pushes the bioink loaded into a syringe through a transparent PTFE microtube in a controllable manner (2). The passage of the microtube inside a low penetrance UV lamp allows the bioink to be exposed to the UV rays for a total of about 8 s (3), which are sufficient to promote bioink polymerization. The cellularized printing fiber extruded through the microtube is finally wrapped around a rotating C-shaped stainless-steel support (4) in order to obtain a bundle of fibers replicating the skeletal muscle native architecture (5). In bulk polymerization, the solution of PF and cells is poured into the Teflon mold in which the C-shaped support is wedged (1). After 5 min UV rays exposure (2), a cellularized bulk construct with the same dimension of the 3D bioprinted construct is obtained (3, 4). Scale bar: 1 cm.

as radical photoinitiator. Irgacure2959 was chosen as photoinitiator of the polymerization reaction due to its low cell toxicity, good performance in photocross-linking hydrogels, and the ability to be solubilized in the aqueous hydrogel precursor solution [21, 22].

## 2.2. Bioprinting system and 3D constructs culture

For this work, a custom-made 3D bioprinter was designed and manufactured. This novel extrusion-based printing system allows to employ PF as only biomaterial of the bioink, and to obtain printing fibers with a high resolution ( $105 \pm 9 \mu\text{m}$ ) forming muscle bundles-like constructs of considerable dimension ( $4 \times 0.2 \times 0.2 \text{ cm}^3$ , figure 1). The core of the system is composed by the printing head that has been optimized to allow the quick polymerization of the bioink (8 s of UV exposure), which occurs during the liquid flow in the inner circuit (a low-attachment PTFE microtube,  $\text{Ø } 300 \mu\text{m}$ ). Liquid bioink is pushed in the circuit by a custom-made syringe pump system at a flow rate of  $100 \mu\text{l min}^{-1}$ . With these parameters, the extrusion printer has a yield of  $60 \text{ cm min}^{-1}$  of printed fiber. The diameter of the extruded printing

fiber ( $300 \mu\text{m}$ , corresponding to the diameter of the inner circuit) is further reduced by the tensile force generated by the rotation of a stainless-steel support (video S1). The C-shape of the support (figure 1) was studied to allow the deposition of parallel, dense and evenly aligned printing fibers with an architecture that closely resembles the native striated muscle bundles. Moreover, an oscillatory ‘forward-reverse’ movement ensures the uniform layer-by-layer distribution of the fibers on the support. The actuation of the printer is provided by stepper motors controlled by an Arduino Uno [[www.arduino.cc](http://www.arduino.cc)] microcontroller board.

Bulk constructs as experimental control were obtained using a Teflon mold with the same dimensions of the printing constructs ( $4 \times 0.2 \times 0.2 \text{ cm}^3$ ). In particular, the C-shaped support was placed in the mold and the liquid bioink was poured in the cavity and polymerized for 5 min, according to the time frame defined during previous optimization [11, 13, 14] under a UV radiation of 365 nm (figure 1). In both bulk and 3D bioprinted constructs production, the time of exposure to

UV rays needed for PF polymerization demonstrated not to affect cell viability, as attested through the Live/Dead Cell Viability Assay Kit (Sigma-Aldrich, figure S1). This analysis also allowed to clarify that the printing process itself does not compromise the survival of the cells included in the bioink.

Bulk and 3D bioprinted constructs were kept in culture in the presence of growth medium and no specific differentiation factors were added as both Mabs and hMSCs are able to spontaneously form myotubes upon reaching 80% confluence. For *in vitro* analysis, constructs were cultured up to 30 d in order to achieve an adequate muscle differentiation. Alternatively, for *in vivo* analysis, constructs were implanted in mice models 48 h after polymerization.

### 2.3. Volumetric muscle loss (VML) model, implants, and sample preparation

The VML murine model was established as previously described [11]. Briefly, two-month-old male SCID/Beige mice were anesthetized with an intramuscular injection of a physiologic saline solution (10 ml kg<sup>-1</sup>) containing ketamine (5 mg ml<sup>-1</sup>) and xylazine (1 mg ml<sup>-1</sup>). After anesthesia, a limited incision was performed on the medial side of the leg to reach the *Tibialis Anterior* (TA). Approximately 90% for mouse-on-mouse implants and 50% for human-on-mouse implants of the total TA muscle volume was removed leaving tendons intact, by using a cautery to avoid bleeding and to create a venue for the implant accommodation (figure S2). The pre-shaped 3D bioprinted construct containing either Mabs or hMSCs was placed (without being sutured) to fill the volume of the surgically ablation that created an anatomic niche and the skin was subsequently sutured. In the control mice, the contralateral TA was surgically ablated, but no construct was implanted.

Analgesic treatment (Rimadyl, Pfizer, USA) was administered after the surgery to reduce pain and discomfort. Mice were sacrificed 30 d after implantation for immuno-histological analyses. Experiments on animals were conducted according to the rules of good animal experimentation I.A.C.U.C. N° 432 of 12 March 2006, and under Italian Health Ministry Approval No. 271/2021-PR.

### 2.4. Sample sectioning and immunofluorescence analysis

At the given time point, 3D constructs were fixed with 4% PFA in PBS for 30 min at 4 °C and subsequently analyzed through immunofluorescence either in whole-mount or after sectioning. The constructs to be processed for sectioning were incubated in solutions with increasing sucrose concentrations (10%, 20% and 30%, 6 h for each concentration), in order to remove most of the water volume and avoid damage during inclusion. Eight micrometers sections were obtained using a Leica cryostat from either fixed constructs or fresh surgical explants through

embedding in OCT resin and quick freezing in liquid nitrogen-cooled isopentane. *In vitro* and *in vivo* resulting samples were accordingly processed for immunofluorescence analysis as previously described [23, 24]. Briefly, samples were permeabilized with 0.3% Triton X-100 in PBS for 1 h at room temperature (RT) and blocked with a blocking solution consisting of 10% goat serum, 1% glycine, 0.1% Triton X-100 in PBS for 1 h at RT. Subsequently, samples were incubated with primary antibodies in blocking solution for 2 h at RT and then rinsed with a washing solution consisting of 1% BSA and 0.2% Triton X-100 in PBS. Primary antibodies were diluted as follows: mouse monoclonal anti-myosin heavy chain (MyHC) (MF20 clone supernatant, DSHB) 1:2, rabbit polyclonal anti-desmin (Abcam) 1:100, rabbit polyclonal anti-laminin (Sigma-Aldrich) 1:200, mouse monoclonal anti-Pax7 (supernatant, DSHB) 1:20, rabbit polyclonal anti-pNF (BioLegend) 1:400, mouse monoclonal anti-SMA (Sigma-Aldrich) 1:100, rabbit polyclonal anti-vWF (Abcam) 1:100, mouse monoclonal anti-Lamin A/C (Thermo Fisher Scientific) 1:200. After washing, cells were incubated with Alexa Fluor 555-conjugated goat anti-mouse IgG (H + L; Thermo Fisher Scientific, diluted 1:400) and 488-conjugated goat anti-rabbit IgG (H + L; Thermo Fisher Scientific, diluted 1:400) for 1 h. Finally, nuclei were stained with 300 nM DAPI (Thermo Fisher Scientific) in PBS for 30 min. When fluorescent-BTX staining was needed,  $\alpha$ -BTX Alexa Fluor 488-conjugated was added to the DAPI solution at a concentration of 1:400. Samples were observed using a Nikon TE 2000 epifluorescence microscope equipped with a Photometrics Cool SNAP MYO CCD camera and images were acquired through MetaMorph® software (Molecular Devices, Inc.). Alternatively, images were acquired through a Nikon A1R laser scanning confocal microscope with the NIS software.

### 2.5. Image analyses

Image analyses were performed by using the ImageJ/FIJI program. Briefly, *in vitro* characterization of spontaneous twitching at day 10 in the bulk and 3D bioprinted constructs was obtained by analyzing the single frames of the live-imaging videos. After properly calibrating images, radial displacement during twitching with respect to a reference point of the image was measured using the Straight Line function [25]. Myofibers size (width and length) was calculated on whole-mount immunofluorescence images using the Straight Line function after image calibration, while coherency was calculated by using the Orientation J plugin, as previously described [11]. To describe fibers density and orientation in the construct cross sections, magnified region of interest (ROI)s were converted in highly contrasted eight-bit images and threshold was applied to generate binary images. After setting the measurements of interest, nuclei area and fibers cross sectional circularity and

area were calculated through the *Analyze Particles* function.

## 2.6. Statistical analysis

All experiments were performed in biological and technical triplicates. Data were analyzed using GraphPad Prism 5, and values were expressed as means  $\pm$  standard error. Statistical significance was tested using a t-test, as only two conditions were compared. A probability of less than 5% ( $p < 0.05$ ) was considered to be statistically significant.

## 3. Results

### 3.1. *In vitro* analysis of myofibers maturation, organization and homogeneity in bioprinted and bulk constructs

The effectiveness of the printing system in sustaining biological processes such as cellular adhesion, proliferation and differentiation was assessed by using murine mesoangioblasts (Mabs). Mabs were added to the bioink composed by PF, a photocurable hydrogel combining natural and synthetic benefit [17]. The obtained bioprinted constructs were maintained in culture up to 30 d, in order to obtain fully differentiated muscle fibers (figure 2(A)). As a parallel experimental control, bulk constructs were polymerized using a Teflon mold with the same dimension of the printing construct (refer to Materials and Methods section, figure 1). In both cases, constructs were kept attached to the C-shaped supports throughout the duration of the experiment in order to have the same passive tension. Interestingly, the effect of shear stress caused by the printing process can be noted by the flat appearance of cells at Day 0 compared to the round shape of cells within the bulk construct (figure 2(A)). Starting from day 10, spontaneous twitching events were recorded in both conditions (video S2). Video frames were analyzed in order to identify any differences in contractile properties in the two conditions. Radial displacement, which indicates the shift occurring during the contraction phase of a single twitch, was significantly higher (2.5-fold) in the bioprinted condition (figure 2(B) and S3). Moreover, a different twitching directionality was observed, being parallel to the printing axis in the bioprinted construct while randomly oriented in the bulk construct (figure 2(B)). At later time points, because of massive spontaneous twitching and the movement of whole constructs, it was not possible to perform video frames quantitative analysis (video S3).

At day 30, upon muscle differentiation, whole-mount immunofluorescence analysis against the muscular differentiation markers MyHC and desmin were performed on both bulk and bioprinted constructs (figure 3(A)). Image analysis confirmed that PF provides a favorable microenvironment for the maintenance of Mabs, able to proliferate and fuse for producing large multinucleated muscle fibers in both

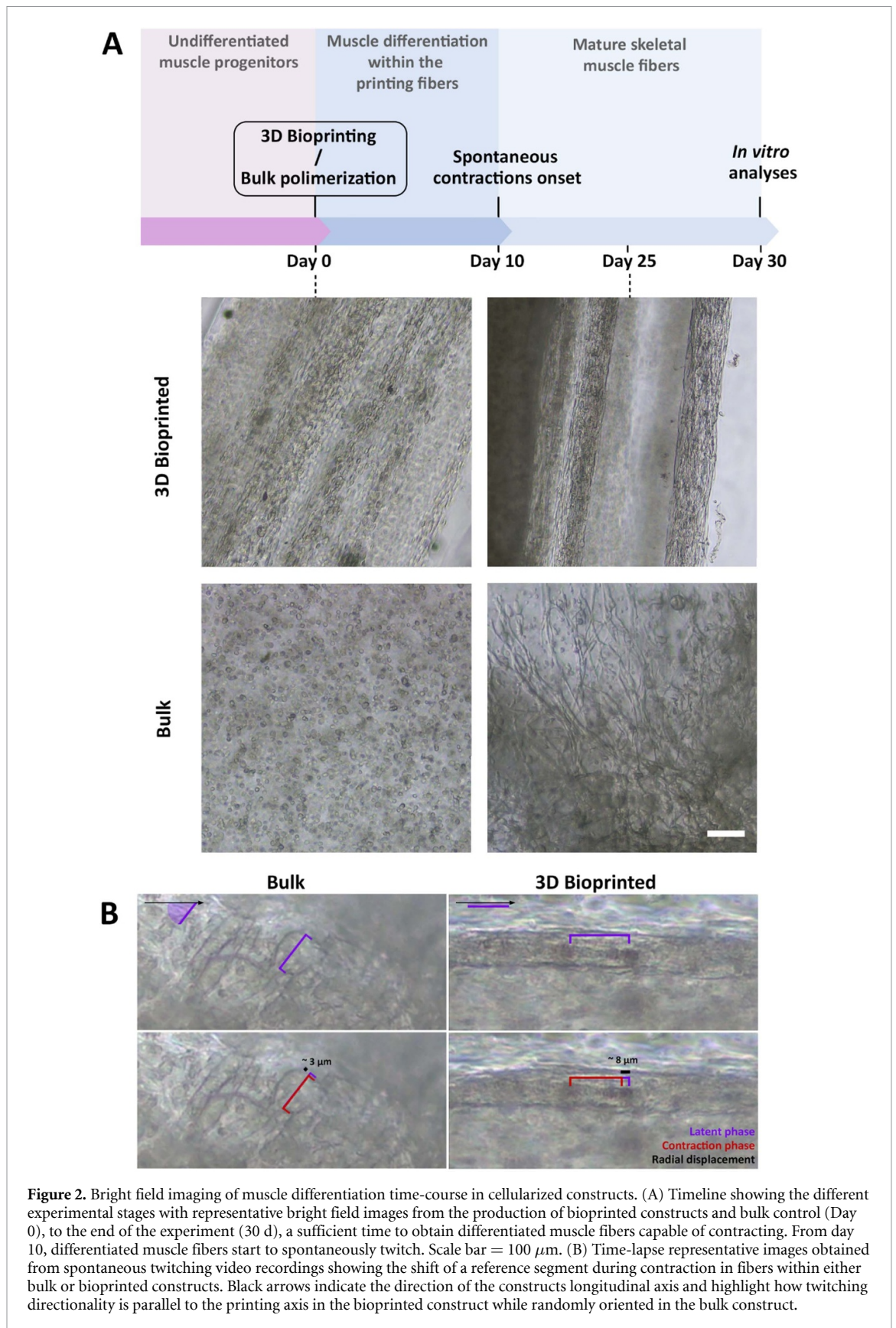
conditions (figure 3(B)). The evidence of a better organization and a greater homogeneity in myofibers size in the bioprinted construct, was assessed by comparing myofibers width, length and coherency in both conditions. Myofibers average width resulted slightly higher in the bioprinted constructs even if not in a statistically significant way (figure 3(C), left). However, the width distribution in the bioprinted construct appeared shifted towards larger dimensions and more peaked as compared to bulk curve (figure 3(C), right). Interestingly, a greater width of fibers could be an indication of a better maturation [26]. Moreover, myofibers average length was significantly higher (two-fold) in bioprinted constructs compared to bulk myofibers, as also confirmed by the shifted length distribution (figure 3(D)). Coherency, a parameter ranging from 0 to 1 and describing the orientation and isotropic properties of analyzed region [27], was found to be significantly higher (3.5-fold) in the bioprinted constructs, with a distribution showing a very pronounced single peak as compared to the flat bulk curve (figure 3(E)).

### 3.2. Analysis of differentiation and fiber alignment on constructs sections

Both bulk and bioprinted constructs were snap frozen for OCT casting to obtain cryo-sections. Immunofluorescence analysis confirmed the presence of desmin-positive and MyHC-positive myofibers in both conditions (figure 4(A), left). Interestingly, cells were able to produce their own extracellular matrix (ECM), as evidenced by the presence of laminin surrounding the fibers and indicating proper maturation (figure 4(A), right). Laminin production is especially visible around centrally nucleated regenerating fibers in bioprinted construct sections (figure 4(A), enlargement). Moreover, significant differences were highlighted by the quantitative analysis of different parameters related to constructs architectural organization. Cellular density, a measurement indicating the presence and the cells localization within the section, is significantly higher in the bioprinted construct reflecting a better distribution of myofibers, whereas in the bulk construct cells localized mainly in the outermost layer (figure 4(B)). Moreover, the circularity and the cross-sectional area measured on the constructs sections resulted respectively higher and lower in the bioprinting condition, indicating the better alignment of myofibers along the construct longitudinal axis (figure 4(C)). On the other hand, the bulk constructs showed a larger cross-sectional area but a lower circularity, as expected for myofibers not oriented in a single direction. (figure 4(D)).

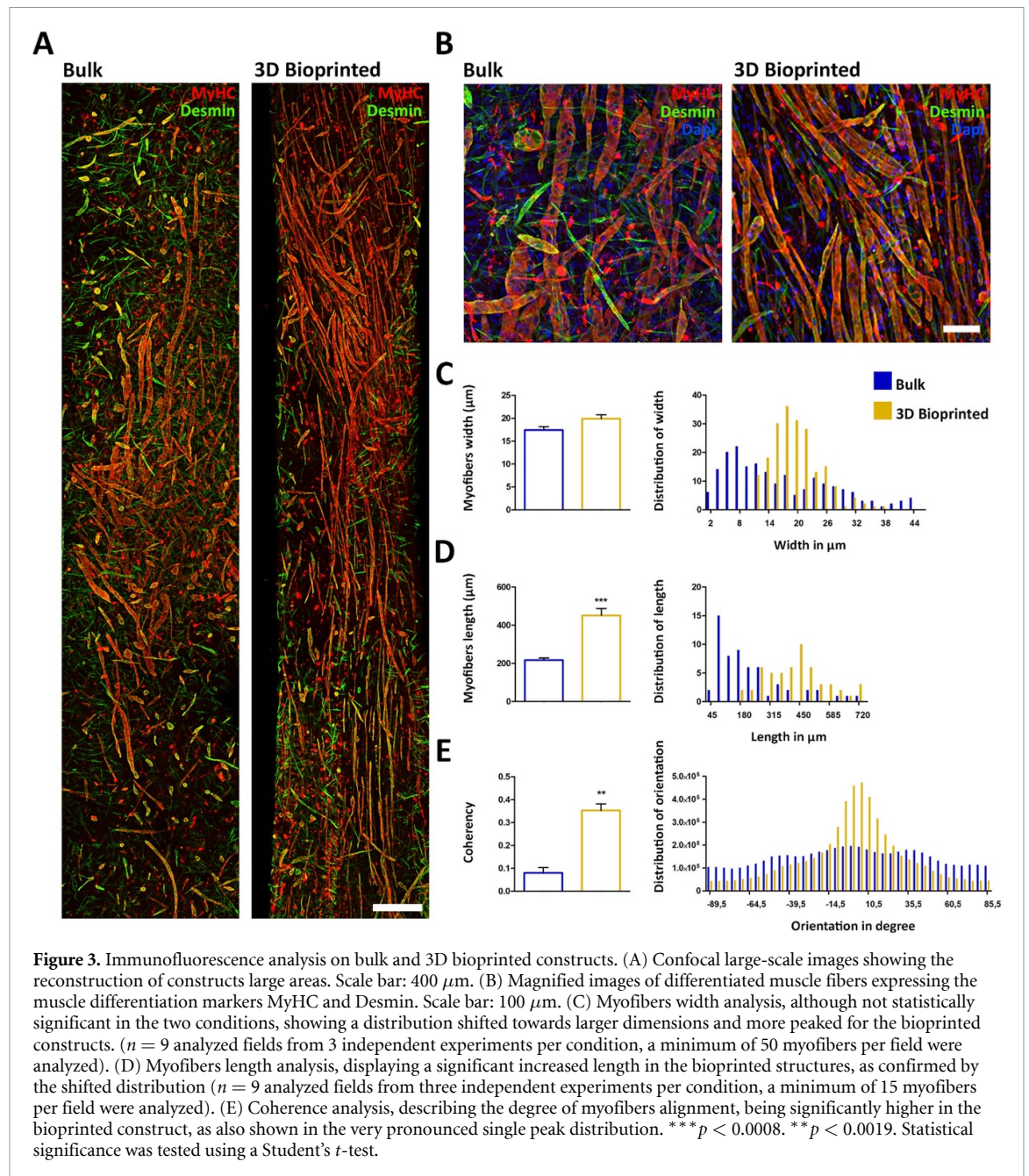
### 3.3. TA volume recovery after murine bioprinted construct implantation

To assess the potentiality of the printing system in regenerative medicine applications, a murine model of VML was employed [11]. The VML



model was obtained by massively ablating (90%) the TA of the mouse hind legs, in order to prevent the natural healing process of the muscle [14]. 3D bioprinted constructs, obtained from nuclear LacZ Mabs (nLacZ-Mabs) [15], were placed

in the anatomical space created by TA removal and the implant was allowed to integrate within the host muscle for 30 d. In the control mice, the TA muscle tissue was ablated without being replaced with the artificial construct. After sacrifice,



ablated and implanted TAs were collected and analyzed through immunofluorescence analysis against laminin and MyHC, while LacZ-positive nuclei were identified by means of X-Gal labeling. The obtained cross sections images revealed the complete recovery of the tissue area in the implanted TA as compared to control, which conversely displayed a poor and deficient tissue restoration (figure 5(A)). A large number of LacZ-positive nuclei were labeled within the centrally nucleated muscle fibers in the reconstructive tissue, which demonstrated to be well organized (figure 5(B) and S4). Reconstructed tissue deriving from the implanted constructs demonstrated to be properly vascularized, as highlighted by the area enriched in LacZ-positive nuclei

showing positive signal for smooth muscle actin (SMA) and von Willebrand factor (vWF), labeling vessel muscle wall and endothelium respectively (figure 6(A)). Moreover, the reconstructed myofibers presenting LacZ-positive nuclei have been shown to be innervated, as demonstrated by the positive labeling of neural pre- and post-synaptic structures by immunostaining with phospho-neurofilament (pNF) and alpha-bungarotoxin (BTX), demonstrating the development of neuromuscular junctions within the regenerating TA muscle, after implantation of 3D constructs (figure 6(B)). Pax7-positive satellite cells were observed in the TA area reconstructed by nLacZ-Mabs, indicating the reestablishment of the stem cell niche required for muscle regeneration (figure 6(C)).

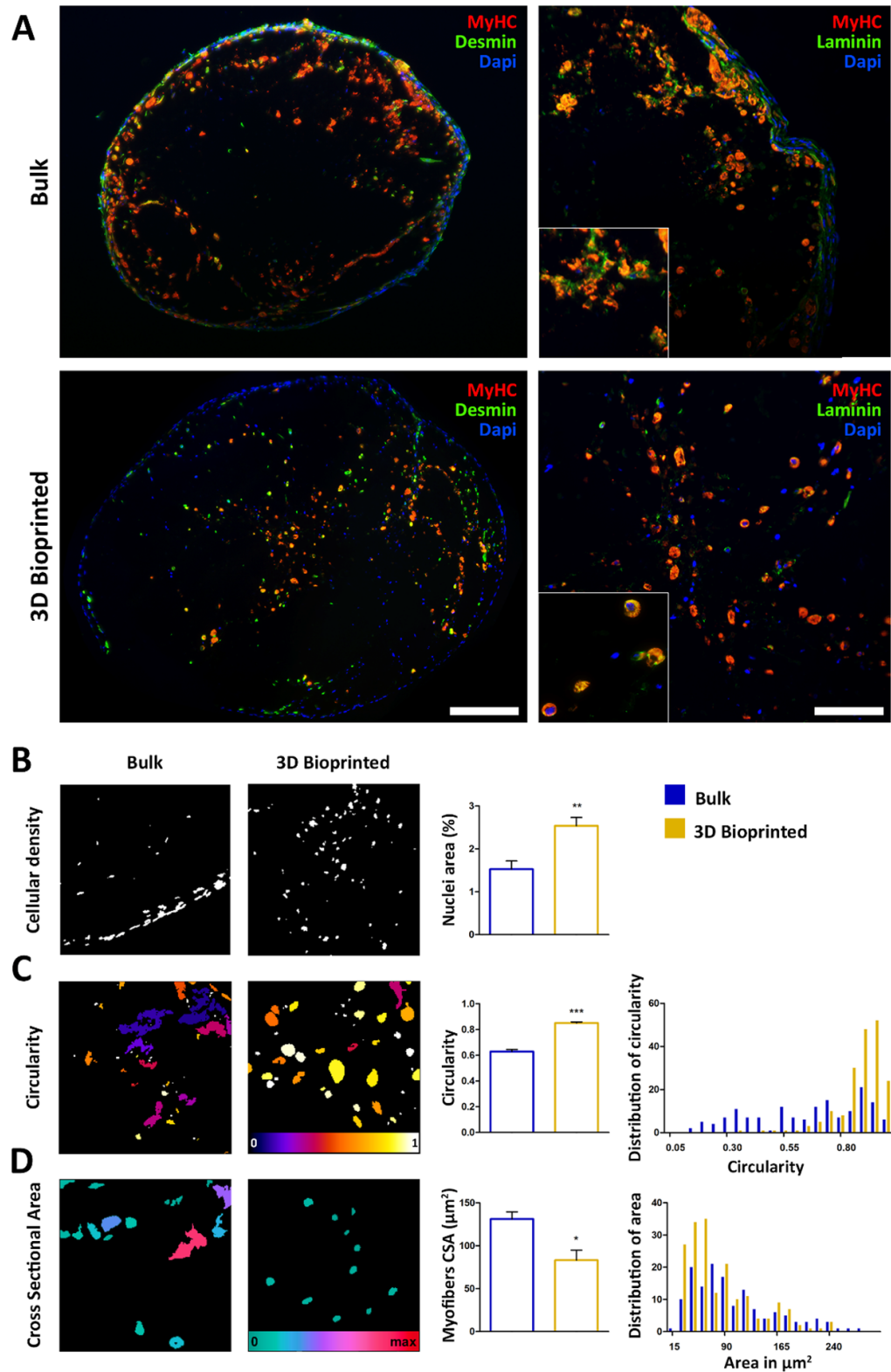


**Figure 4.** Analysis of the constructs cross sections. (A) Cross sections of bulk and bioprinted constructs confirming the expression of the muscle differentiation markers MyHC and desmin (left) and the production of laminin-positive extracellular matrix (right), which is particularly noticeable around centrally nucleated transverse fibers in the bioprinted construct (enlargements). Left scale bar: 200  $\mu\text{m}$ , right scale bar: 100  $\mu\text{m}$ . Cellular density (B), which is expressed through nuclei percentage area, and alignment (C), which is expressed through circularity, resulted significantly higher in the bioprinted condition. Moreover, myofibers cross sectional area (D) resulted significantly higher in the control, as a result of a greater myofibers inclination.  $**p < 0.0041$ .  $***p < 0.0001$ .  $*p < 0.0296$ . Statistical significance was tested using Student's *t*-test.

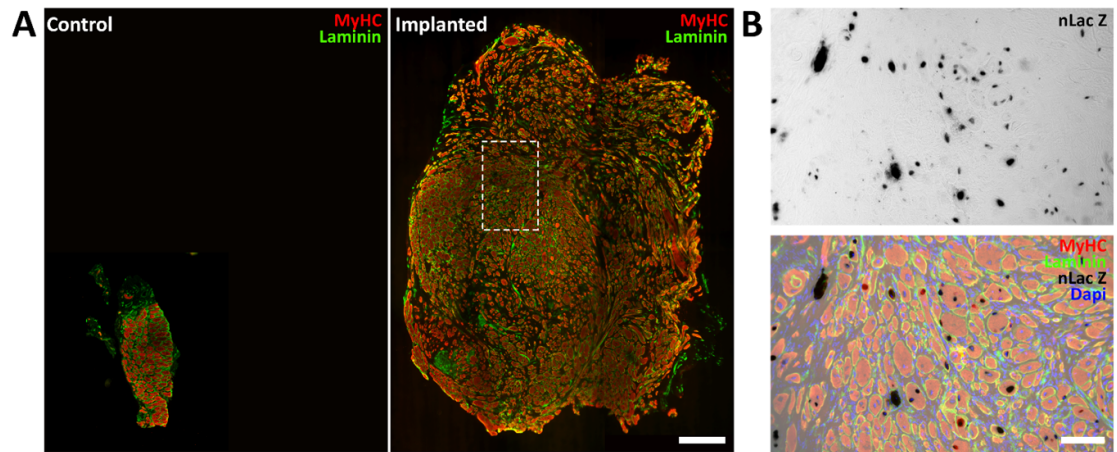


**Figure 5.** Immunofluorescence analysis on ablated and implanted murine TAs. (A) Cross sections images analyzed through immunofluorescence analysis against laminin and MyHC revealed a complete area recovery of the TA implanted with the nLacZ-Mabs-laden bioprinted construct as compared to the ablated control. Scale bar: 400  $\mu\text{m}$ . (B) Magnified images of the area dashed in A showing LacZ-positive nuclei, labeled by X-Gal assay. Scale bar: 100  $\mu\text{m}$ .

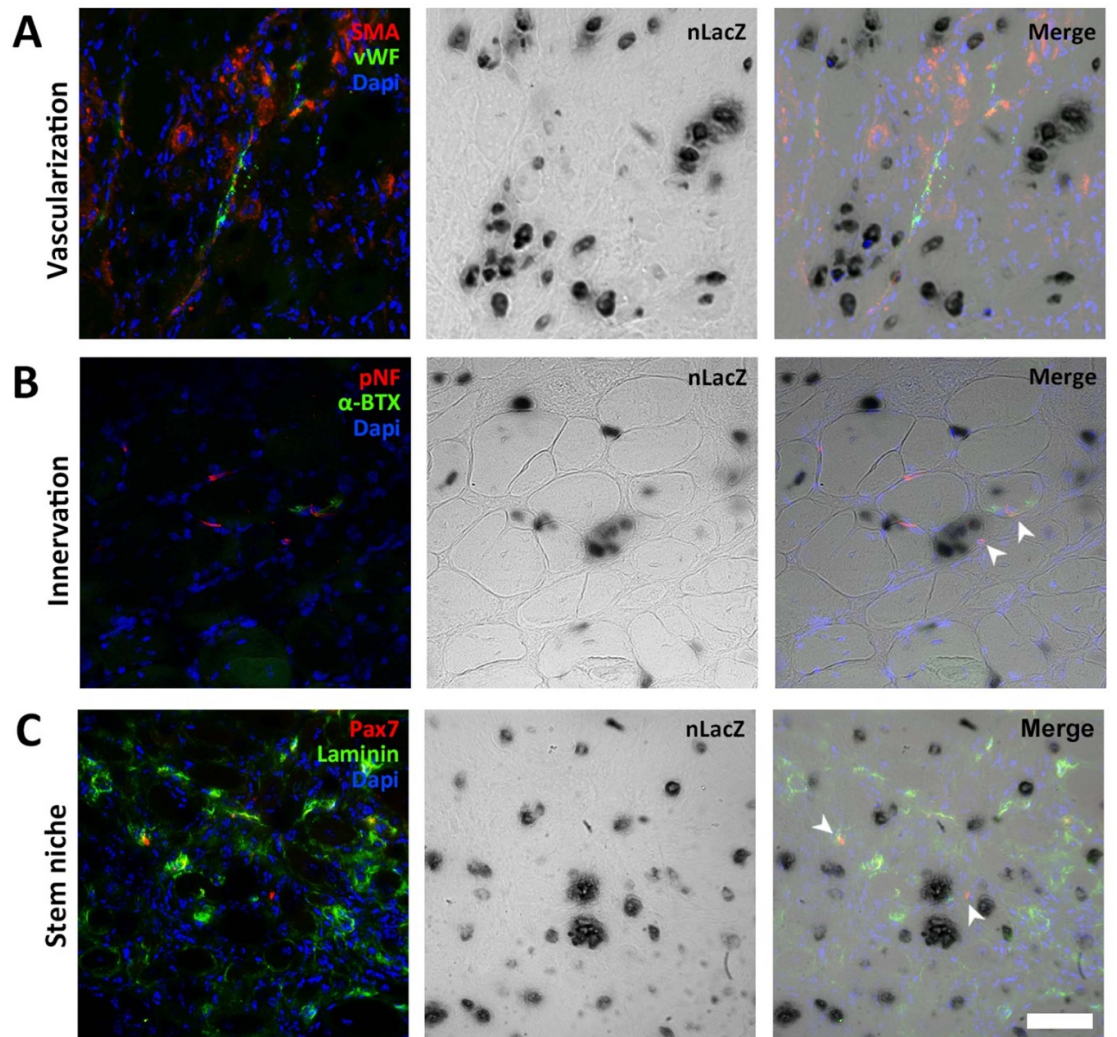


**Figure 6.** Higher magnifications analysis of the area regenerated by nLacZ-Mabs in 3D bioprinted constructs. (A) Immunofluorescence analysis against vessels-specific markers SMA and vWF indicate proper vascularization of the regenerating area. (B) Labeling by means of immunofluorescence for the pre- and post-synaptic neural markers pNF and BTX, targeting neurons cytoskeleton and muscular acetylcholine receptors, respectively. White arrowheads highlight developing fibers with central LacZ-positive nuclei showing host nerve terminals. (C) Pax7-positive satellite cells indicated by white arrowheads detected in LacZ-positive nuclei-rich area. Scale bar: 50  $\mu\text{m}$ .

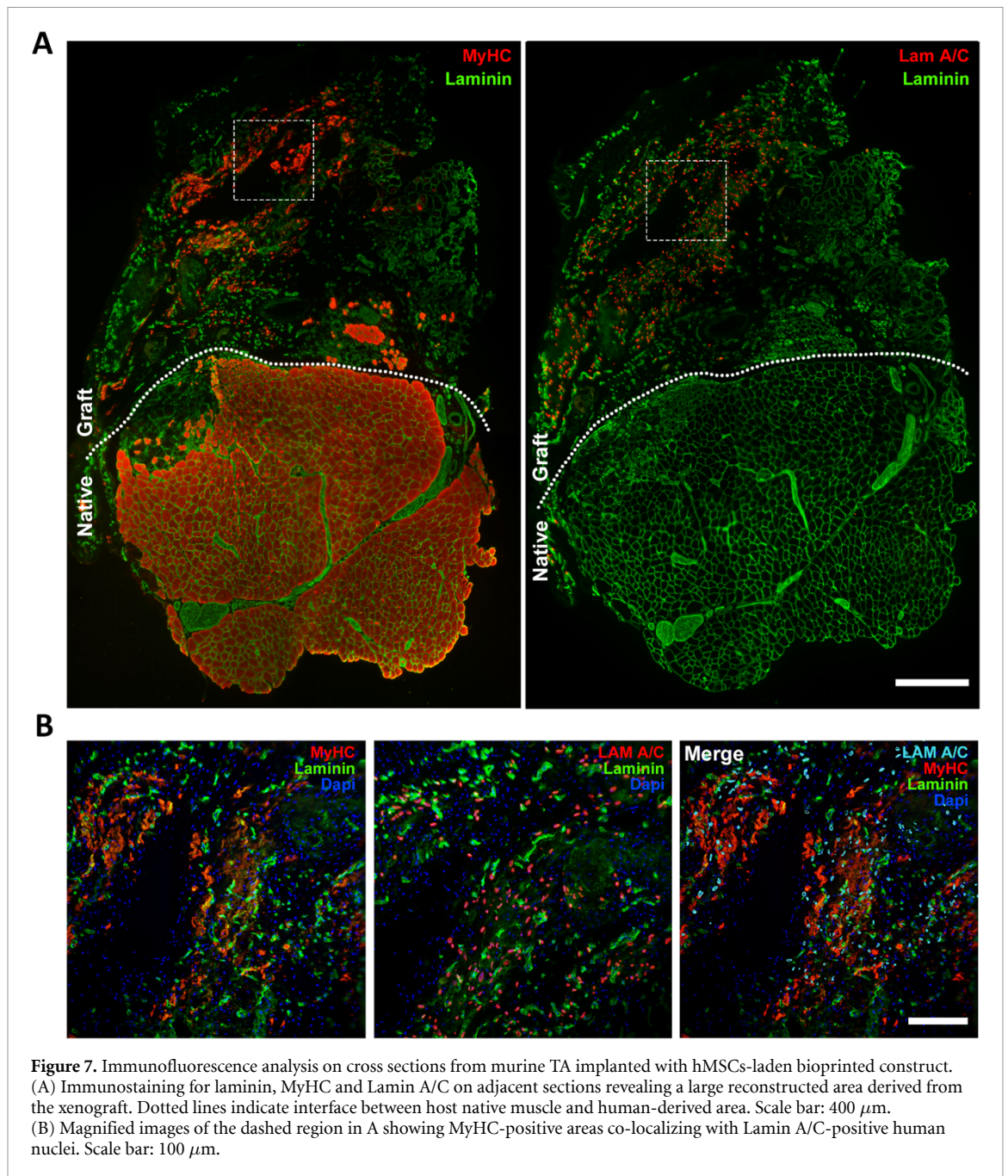
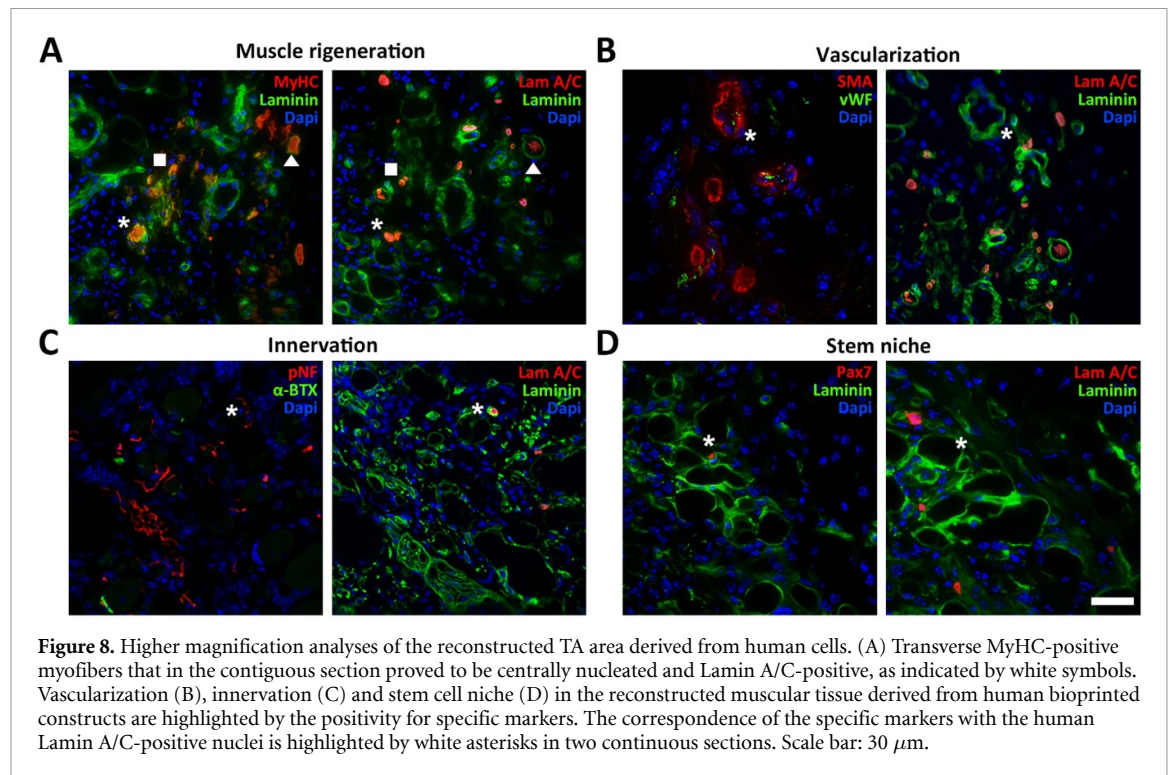


**Figure 7.** Immunofluorescence analysis on cross sections from murine TA implanted with hMSCs-laden bioprinted construct. (A) Immunostaining for laminin, MyHC and Lamin A/C on adjacent sections revealing a large reconstructed area derived from the xenograft. Dotted lines indicate interface between host native muscle and human-derived area. Scale bar: 400  $\mu\text{m}$ . (B) Magnified images of the dashed region in A showing MyHC-positive areas co-localizing with Lamin A/C-positive human nuclei. Scale bar: 100  $\mu\text{m}$ .

### 3.4. TA volume recovery after human bioprinted construct implantation

In order to evaluate the possibility to translate the proposed approach in human studies, pilot experiments have been performed exploiting muscle-derived hMSCs-laden bioprinted constructs. For this purpose, constructs with human cells were implanted in the mouse hind limb upon 50% TA muscle ablation, similarly to the above-described experiment. After 30 d, tissues were collected and analyzed by means of immunofluorescence. Cross sections of the explanted TA show two distinct areas, one being the host native muscle and the other one resulting from the human-derived bioprinted implant (figure 7(A)). Although the tissue developed from the xenograft seems overall less organized compared with the

murine-derived implants (figure 5), the large MyHC-positive area co-localizing with numerous human Lamin A/C (Lam A/C)-positive nuclei indicate that the reconstructed muscular tissue is from human origin and that hMSCs were able to generate myofibers integrating with host ablated TA (figure 7(B)). Interestingly, a deeper analysis of the reconstructed TA tissue showed more organized areas with transverse small muscle fibers that in the contiguous section proved to be centrally nucleated and Lamin A/C-positive (figure 8(A)). Tissue reconstituted from the human-derived implant has shown also to be properly vascularized and innervated, as highlighted by the positive signal revealed by vessels- (SMA and vWF) and neural-specific (pNF and BTX) markers (figures 8(B) and (C)). Moreover, the presence of



Pax7-positive satellite cells was observed in the periphery of some fibers, thereby suggesting the regenerative potential of the reconstructed TA (figure 8(D)).

#### 4. Discussion

To date, 3D bioprinting approach is gaining more and more interest for its ability to produce cellularized 3D constructs with a well-defined architecture closely replicating tissue organization in a quick and highly reproducible manner [28–31]. However, regardless of the printing system, this target often proves challenging. Indeed, the technical requirements of 3D printing combined with the necessity for a biocompatible cellular scaffold force researchers to find a compromise in formulating bioink between what is convenient for the machine and what is suitable for cell survival, proliferation and differentiation. Several research groups have faced these hurdles, investigating different strategies based on multi-component bioinks and/or multi-step polymerization processes. In particular, good outcomes have been obtained with PEG-Chitosan, Gelatin and porcine decellularized ECM [28, 30, 31]. However, existing approaches often require a difficult set-up involving considerable changes of temperature during the extrusion process and the combination of chemical/physical polymerization of the bioink, while at the same time not providing a resolution of less than 300  $\mu\text{m}$ .

Our team also focused its efforts on this direction, basing the bioink formulation on the combination of alginate and PF, in order to exploit alginate printability together with PF biological compatibility.

With this approach, the bioink was transiently reticulated during the printing process by exposing the alginate to a covalent ions solution, while irreversible polymerization was achieved in a second step by UV exposure that acts on PF molecules. Subsequently, the alginate was removed from the scaffold with a calcium chelating agent or an alginate enzyme solution. This technique demonstrated optimal outcomes *in vitro*, allowing differentiation of muscle progenitor cells and production of highly organized muscle constructs. However, in VML regeneration experiments, alginate residues remained in the constructs affected the quality of the resulting muscle [11, 13].

In an attempt to overcome these limitations, this work further described a novel and versatile alginate-free and extrusion-based 3D bioprinting system. The development of the proposed printing system is based on the characteristics of PF, a hydrogel able to sustain growth and differentiation of skeletal muscle cells both *in vivo* and *in vitro* [15, 16]. In this way, instead of formulating the right biomaterial according to the printing system features, priority was given to the cell physiological requirements. Initially, PF physical properties did not seem compatible with a printing system based on the use of this hydrogel only, as the polymerization time is relatively long (5 min of UV rays exposure). For this reason, the printer features have been customized in order to drastically reduce the PF polymerization time to 8 s, allowing a rapid and cell-friendly printing process. Another strength of the presented bioprinter is the C-shaped stainless-steel support, specifically designed to allow the production of 3D constructs composed by fibers bundles

similar to the skeletal muscle tissue architecture. The use of a linear support allows to collect the printing fibers in highly aligned lines between the two pins and to produce an elongated bundle, representing an improvement over the circular constructs obtained with cylindrical supports [11]. Notably, rotation of the C-shaped support pulls the printing fibers and leads to an increase of the printing resolution to 100  $\mu\text{m}$  (1/3 of the extruder microtube diameter). Moreover, a translational 'forward-reverse' movement allows the layer-by-layer deposition of printing fibers on the support, so as to recapitulate muscle organization.

The potential of the PF-based bioprinting system in supporting the biological processes needed for muscle differentiation has been evaluated using murine mesoangioblasts (Mabs) as the source of muscle progenitors [15]. Our results confirmed PF as an ideal scaffold for the growth, differentiation and maturation of muscle fibers, which have been shown to be able to twitch spontaneously both in bioprinted and bulk condition. A difference in the myofibers overall organization between the two conditions emerged from the first brightfield analyses, and the formation of differentiated and aligned myofibers in the bioprinted constructs demonstrated to be necessary to the coherent muscle bundles contraction. Moreover, with the aim of identifying differences in the contracting behavior of myofibers within bulk and bioprinted constructs, we recorded and described a greater radial displacement during the contraction phase of the bioprinted myofibers. Taking into account the relationship between myofibers size and their ability to generate force [32], we speculate this result might indicate an ability to produce a greater amount of force as compared to the twitching myofibers of the bulk construct. Shear stress and geometric confinement induced by 3D bioprinting confirmed to have an influence on the elongation and alignment of homogeneous muscle fibers. Moreover, cross sections showed how bioprinting promotes a more homogeneous myofibers distribution within the construct as compared to the bulk condition, in which muscle fibers are arranged only in the most external layer. We speculate that this phenomenon could be the result of an improved oxygen and medium perfusion through the space between the printing fibers.

Relying on the encouraging results obtained *in vitro*, we proceeded investigating the capability of the constructs obtained with the proposed bioprinting system in restoring a VML in a murine model. VML, resulting from severe trauma or sarcomas surgical ablation, is a pathological condition that prevents the regeneration of skeletal muscle, as it owns considerable ability to repair tissue damage but only when limited in size [33]. Unfortunately, currently adopted surgical therapies do not yet provide satisfactory results. To date, one of the most widely

employed clinical strategy for the treatment of VML trauma is the implantation of acellularized scaffolds composed by ECM often derived from natural sources (e.g. porcine urinary bladder-derived ECM). However, the functional recovery is limited, making this reconstructive therapy inadequate [24]. For this reason, an increasing attention is being paid to skeletal muscle tissue engineering as a promising approach.

In our experiments, 3D bioprinted Mabs-laden constructs lead to a full restoration of the lost muscle volume 30 d after grafting. The acellular PF bioprinted construct was not employed as experimental control for implantation experiments, as it has already well demonstrated to be completely reabsorbed by the host organism in previous papers [11, 14]. The wide implantation of Mabs in the regenerating tissue (figure S4) indicates an active role of the implant not only in the regeneration of muscle fibers, but also in driving the recruitment of all the biological elements required for implant survival and for proper development of a functional muscle tissue. Functional recovery rate will be the focus of future studies.

Finally, as a proof-of-concept to evaluate the translational potential of the proposed approach, hMSCs [19] were employed to obtain 3D bioprinted constructs. A less extensive VML (50% TA volume ablation) was chosen for these experiments, based on our previous experiences with human-on-mouse grafts where the host did not fully accept the human cells (data not shown). Similarly to murine experiments, 30 d after implantation the human cell-derived bioprinted constructs were able to restore the host muscle volume even if the reconstructed tissue was not fully organized as for Mabs-derived implant (mouse-on-mouse). However, a large number of human cells survived in the host and were able to drive the formation of new muscle fibers, to recruit blood vessels and nerves, and to stimulate the formation of a pool of satellite cells. Altogether, the presented data make us confident that the proposed reconstructive strategy has the potential to be suitable for future translational medicine application in human.

## 5. Conclusion

In this work, the proposed alginate-free extrusion-based 3D bioprinting system, established on the use of PF as only hydrogel composing the cellular scaffold, demonstrated to be a novel and competitive tool for skeletal muscle tissue engineering. The bioprinter was developed by exploiting our expertise, acquired over the years, on skeletal muscle tissue engineering and on the use of the most suitable hydrogels for myogenesis. This background granted us to realize a simple yet effective strategy to overcome limitations of previous systems that depend on the combination of PF with other less biocompatible hydrogels (such as alginate). The presented results highlighted the potential of this

innovative printing approach in two main aspects: on one hand, the possibility to obtain *in vitro* biological substitutes showing properly organized muscle fibers capable of spontaneously contracting, which could represent a biological platform for drug screening and myopathies studies. On the other hand, the efficacy of the printed construct in restoring a VML damage in a mouse model, both with murine and human-derived myogenic progenitors, suggesting that the proposed approach could represent a remarkable and effective tool for regenerative medicine.

Finally, the ease-of-use the presented approach could lend itself to the use of other photo-curable biomaterials (such as gelatin and other PEG-based hydrogels) and different types of mesodermal stem cells (Bone Mesenchymal Stem Cells [34, 35], Adipose-derived Stem Cells [36], Tendon-derived Stem Cells [37]) to print a wide range of mesodermal-derived tissues as 3D models or transplantable substitute.

### Data availability statement

All data that support the findings of this study are included within the article (and any supplementary files).

### Acknowledgments

We thank Massimo Testa for the support in designing and manufacturing the 3D bioprinter system and Dr Franca Abbruzzese (Università Campus Bio-Medico di Roma) for her technical support on confocal microscopy acquisition. The research has been carried out thanks to PRIN 2017: 201742SBXA\_004 funded by Italian Ministry of University and Research to Cesare Gargioli.

### Conflict of interest

The authors declare no conflict of interest.

### ORCID iDs

E Fornetti  <https://orcid.org/0000-0002-6246-5351>  
A Rainer  <https://orcid.org/0000-0001-8971-551X>

### References

- [1] Fan T, Wang S, Jiang Z, Ji S, Cao W, Liu W, Ji Y, Li Y, Shyh-Chang N and Gu Q 2022 Controllable assembly of skeletal muscle-like bundles through 3D bioprinting *Biofabrication* **14** 015009
- [2] Kim J H, Seol Y J, Ko I K, Kang H W, Lee Y K, Yoo J J, Atala A and Lee S J 2018 3D bioprinted human skeletal muscle constructs for muscle function restoration *Sci. Rep.* **8** 12307
- [3] Aubin H, Nichol J W, Hutson C B, Bae H, Sieminski A L, Cropek D M, Akhyari P and Khademhosseini A 2010 Directed 3D cell alignment and elongation in microengineered hydrogels *Biomaterials* **31** 6941–51
- [4] Kim W J and Kim G H 2020 3D bioprinting of functional cell-laden bioinks and its application for cell-alignment and maturation *Appl. Mater. Today* **19** 100588
- [5] Naghieh S and Chen X 2021 Printability—a key issue in extrusion-based bioprinting *J. Pharm. Anal.* **11** 564–79
- [6] Fu Z, Naghieh S, Xu C, Wang C, Sun W and Chen X 2021 Printability in extrusion bioprinting *Biofabrication* **13** 033001
- [7] Hospodiuk M, Dey M, Sosnoski D and Ozbolat I T 2017 The bioink: a comprehensive review on bioprintable materials *Biotechnol. Adv.* **35** 217–39
- [8] Croisier F and Jérôme C 2013 Chitosan-based biomaterials for tissue engineering *Eur. Polym. J.* **49** 780–92
- [9] Ferreira A M, Gentile P, Chiono V and Ciardelli G 2012 Collagen for bone tissue regeneration *Acta Biomater.* **8** 3191–200
- [10] Willson K, Atala A and Yoo J J 2021 Bioprinting au naturel: the biologics of bioinks *Biomolecules* **11** 1593
- [11] Costantini M et al 2021 Biofabricating murine and human myo-substitutes for rapid volumetric muscle loss restoration *EMBO Mol. Med.* **13** 1–17
- [12] Wang X, Li X, Dai X, Zhang X, Zhang J, Xu T and Lan Q 2018 Coaxial extrusion bioprinted shell-core hydrogel microfibers mimic glioma microenvironment and enhance the drug resistance of cancer cells *Colloids Surf. B* **171** 291–9
- [13] Costantini M et al 2017 Microfluidic-enhanced 3D bioprinting of aligned myoblast-laden hydrogels leads to functionally organized myofibers *in vitro* and *in vivo* *Biomaterials* **131** 98–110
- [14] Fuoco C et al 2015 *In vivo* generation of a mature and functional artificial skeletal muscle *EMBO Mol. Med.* **7** 411–22
- [15] Fuoco C et al 2012 Injectable polyethylene glycol-fibrinogen hydrogel adjuvant improves survival and differentiation of transplanted mesoangioblasts in acute and chronic skeletal-muscle degeneration *Skelet. Muscle* **2** 24
- [16] Fuoco C et al 2014 3D hydrogel environment rejuvenates aged pericytes for skeletal muscle tissue engineering *Front. Physiol.* **5** 203
- [17] Almany L and Seliktar D 2005 Biosynthetic hydrogel scaffolds made from fibrinogen and polyethylene glycol for 3D cell cultures *Biomaterials* **26** 2467–77
- [18] Buonvino S, Ciocci M, Seliktar D and Melino S 2021 Photo-polymerization damage protection by hydrogen sulfide donors for 3D-cell culture systems optimization *Int. J. Mol. Sci.* **22** 6095
- [19] Testa S et al 2020 Skeletal muscle-derived human mesenchymal stem cells: influence of different culture conditions on proliferative and myogenic capabilities *Front. Physiol.* **11** 553198
- [20] Schaefer B, Beier J P and Ruhl T 2020 Mesenchymal stem cells and the generation of neomuscle tissue *Surg. Technol. Int.* **36** 41–47
- [21] Bryant S J, Nuttelman C R and Anseth K S 2000 Cytocompatibility of UV and visible light photoinitiating systems on cultured NIH/3T3 fibroblasts *in vitro* *J. Biomater. Sci. Polym. Ed.* **11** 439–57
- [22] Mironi-Harpaz I, Wang D Y, Venkatraman S and Seliktar D 2012 Photopolymerization of cell-encapsulating hydrogels: crosslinking efficiency versus cytotoxicity *Acta Biomater.* **8** 1838–48
- [23] Testa S, D'Addabbo P, Fornetti E, Belli R, Fuoco C, Bernardini S, Cannata S, Frezza D and Gargioli C 2018 Myoblast myogenic differentiation but not fusion process is inhibited via MyoD tetraplex interaction *Oxid. Med. Cell. Longev.* **2018** 7640272
- [24] Testa S, Fornetti E, Fuoco C, Sanchez-Riera C, Rizzo F, Ciccotti M, Cannata S, Sciarra T and Gargioli C 2021 The war after war: volumetric muscle loss incidence, implication, current therapies and emerging reconstructive strategies, a comprehensive review *Biomedicines* **9** 564

- [25] Chandel I, Baker R, Nakamura N and Panin V 2020 Live imaging and analysis of muscle contractions in *Drosophila* embryo *J. Vis. Exp.* **9**
- [26] Bakooshli M A *et al* 2019 A 3D culture model of innervated human skeletal muscle enables studies of the adult neuromuscular junction *Elife* **8** 1–29
- [27] Clemons T D, Bradshaw M, Toshniwal P, Chaudhari N, Stevenson A W, Lynch J, Fear M W, Wood F M and Iyer K S 2018 Coherency image analysis to quantify collagen architecture: implications in scar assessment *RSC Adv.* **8** 9661–9
- [28] Hu T, Cui X, Zhu M, Wu M, Tian Y, Yao B, Song W, Niu Z, Huang S and Fu X 2020 3D-printable supramolecular hydrogels with shear-thinning property: fabricating strength tunable bioink via dual crosslinking *Bioact. Mater.* **5** 808–18
- [29] Ostrovidov S *et al* 2019 Three dimensional bioprinting in skeletal muscle tissue engineering *Small* **15** 1805530
- [30] Kim W, Lee H, Lee J, Atala A, Yoo J J, Lee S J and Kim G H 2020 Efficient myotube formation in 3D bioprinted tissue construct by biochemical and topographical cues *Biomaterials* **230** 119632
- [31] Hwangbo H, Lee H, Jin E J, Lee J Y, Jo Y, Ryu D and Kim G H 2022 Bio-printing of aligned GelMa-based cell-laden structure for muscle tissue regeneration *Bioact. Mater.* **8** 57–70
- [32] Cooper A N, McDermott William J, James C Martin, Dulaney Shea O and Carrier D R 2021 Great power comes at a high (locomotor) cost: the role of muscle fascicle length in the power versus economy performance trade-off *Exp. Biol.* **224**
- [33] Corona B T, Garg K, Ward C L, McDaniel J S, Walters T J and Rathbone C R 2013 Autologous minced muscle grafts: a tissue engineering therapy for the volumetric loss of skeletal muscle *Am. J. Physiol. Cell Physiol.* **305** 761–75
- [34] Bae S W, Lee K W, Park J H, Lee J H, Jung C R, Yu J J, Kim H Y and Kim D H 2018 3D bioprinted artificial trachea with epithelial cells and chondrogenic-differentiated bone marrow-derived mesenchymal stem cells *Int. J. Mol. Sci.* **19** 1–14
- [35] Luo C, Xie R, Zhang J, Liu Y, Li Z, Zhang Y, Zhang X, Yuan T, Chen Y and Fan W 2020 Lowerature three-dimensional printing of tissue cartilage engineered with gelatin methacrylamide *Tissue Eng. C* **26** 306–16
- [36] Stanco D, Boffito M, Bogni A, Puricelli L, Barrero J, Soldati G and Ciardelli G 2020 3D bioprinting of human adipose-derived stem cells and their tenogenic differentiation in clinical-grade medium *Int. J. Mol. Sci.* **21** 1–23
- [37] Lui P P Y and Chan K M 2011 Tendon-derived stem cells (TDSCs): from basic science to potential roles in tendon pathology and tissue engineering applications *Stem Cell Rev. Rep.* **7** 883–97